Available online at www.sciencedirect.com

ScienceDirect

Procedia CIRP 58 (2017) 25 – 30

www.elsevier.com/locate/procedia

16th CIRP Conference on Modelling of Machining Operations

Thermomechanical coating load in dependence of fundamental coating properties

S. Beblein[a,*], B. Breidenstein[a], B. Denkena[a], C. Pusch[b], H. Hoche[b], M. Oechsner[b] *

[a]*Institute of Production Engineering and Machine Tools (IFW), Leibniz Universität Hannover, An der Universität 2, D-30823 Garbsen, Germany*
[b]*State Materials Testing Laboratory (MPA), Institute for Materials Technology (IfW), Technische Universität Darmstadt, Grafenstr. 2, D-64283 Darmstadt, Germany*

* Corresponding author. Tel.: +49-511-762-18262; fax: +49-511-762-5115. *E-mail address:* beblein@ifw.uni-hannover.de

Abstract

The conventional development of a coating system for cutting tools includes a variety of test series with elaborate experimental parameter studies. In particular, experimental investigations of the cutting behavior cause a significant consumption of cost, time and resources. In order to adapt the coating properties to the specific requirements of the cutting process, it is desirable to reduce the experimental effort of coating development by simulation of the machining process. Therefore, the main factors of the thermo-mechanical coating load in machining AISI 4140 were identified by means of 2D FEM chip formation simulations. In order to provide the required thermal and mechanical coating properties for the simulations, CrAlN-based coatings were deposited onto cutting inserts and extensively characterized. Within the simulations, the coating properties were varied between the physical and technological boundaries of CrAlN-based coatings. It was shown that the Young's modulus, the coating thickness and the friction coefficient significantly influence the thermomechanical load and the stress distribution within the coating. Finally, the cutting performance of the coated inserts was experimentally investigated and compared with the results of the simulations. Here, it was shown that delamination of the coating is particularly influenced by coating thickness.

Peer-review under responsibility of the scientific committee of The 16th CIRP Conference on Modelling of Machining Operations

Keywords: Machining; Coating; Chip formation simulation

1. Introduction

A coating specifically tailored to the cutting process can significantly increase the performance of cutting tools [1]. Particularly in the case of dry machining, the cutting tools are exposed to high thermomechanical loads. As an industrially widespread coating for dry machining, monolayer and multilayer hard compound coatings based on (Ti,Al)N are used on cemented carbide substrates [1]. As an alternative to Ti-based coating systems, highly heat- and oxidation-resistant ternary und multinary coatings such as CrAlN, CrAlSiN and (Cr,Al,Y)N are increasingly becoming the focus of research [2,3,4]. Despite the high hot hardness and oxidation resistance, CrAlN-based coatings have not yet become established in continuous turning processes. Especially for CrAlN-based coatings the relationships between coating properties and resulting load as well as the wear behavior are not sufficiently known. Furthermore, there are no methods for determining the resulting stresses in the coating during machining. The analysis of the fundamental interrelationship between coating properties and resulting wear in machining with coated cutting tools could enable the development of application-specific CrAlN-based coating systems, which meet the requirements of the dry turning process. In order to reduce the experimental effort within the coating development, simulative approaches are increasingly used [5,6,7]. Therefore, in the present paper the influence of various coating properties on the thermomechanical load of CrAlN-coated cemented carbide tools during machining of AISI 4140 is investigated by means of the finite element method. Finally, the simulations are compared with the cutting performance in experimental turning tests.

Peer-review under responsibility of the scientific committee of The 16th CIRP Conference on Modelling of Machining Operations
doi:10.1016/j.procir.2017.03.184

2. Coating technology and substrate characterization

CrAlN-based coatings were deposited onto WC-Co cemented carbide inserts (Ceratizit CTS12D, SNUN120412EN) using an industrial PVD magnetron sputter unit CemeCon CC800/9. For the deposition two target concepts were used: On the one hand the CrAlN coatings were deposited by reactive magnetron sputtering of two chromium and two aluminum targets using nitrogen as reactive gas. On the other hand four segmented targets with chromium and aluminum segments were used. Furthermore, CrAlYN and CrAlSiN coatings were deposited by additional use of yttrium and silicon segments, respectively. The properties of the inserts, based on data from the manufacturer, are summarized in Table 1.

Table 1. Substrate properties

Density [ISO 3369]	14.8 g/cm³
Hardness HV30 [ISO 3878]	1820
Young's modulus [ISO 3312]	624 GPa
Transverse Rupture Strength [ISO 3327]	3600 MPa
Compressive Strength [ISO 4506]	7000 MPa
Grain Size Classification [ISO 4499]	submicron
Chemical Composition: WC: 93.25 wt%, Co: 6 wt%, Additives: 0.75 wt%	

To ensure a sufficient coating adhesion the substrates were subject to a pretreatment. This included microblasting, wet-chemical cleaning and plasma etching. In order to supply the cutting simulation with accurate thermal properties of the substrate, the specific heat capacity and the thermal expansion coefficient were determined experimentally (Fig. 1). However, thermal conductivity is based on data from the manufacturer.

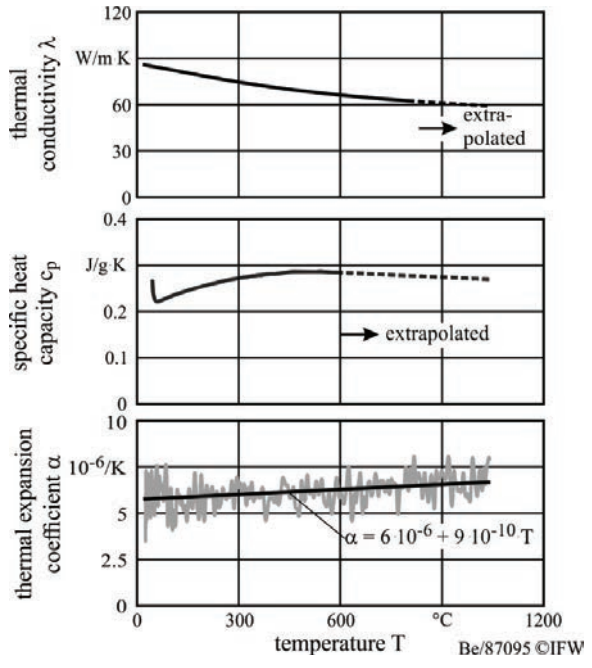

Fig. 1. Thermal properties of the substrate.

The specific heat capacity was measured by means of differential scanning calorimetry (DSC) using the calorimeter Netzsch DSC 200F3. Therefore, a section of the insert material was heated from 40 °C to 600 °C with a heating rate of 10 K/min. Sapphire was used as a reference material. The evaluation was done according to DIN 51007. The thermal expansion coefficient was determined according to DIN 51045 by means of dilatometry using a Netzsch DIL 402E dilatometer. Therefore, the change in length was determined after heating a section of the inserts from 20 °C to 1100 °C with a heating rate of 10 K/min. Al_2O_3 was used as reference material for the correction. A linear function for the thermal expansion was assumed for the simulation. Since high temperatures can occur particularly in the case of dry machining, the values for the thermal conductivity and the specific heat capacity have been extrapolated to 1100 °C.

3. Coating characterization

The coated specimens were characterized in order to supply the cutting simulation with the physical and mechanical coating properties. Since the influence of the material properties on the thermomechanical load is the focus of this work, the relationship between the parameters of the coating process and the coating properties is not discussed in this paper. The hardness and the Young's modulus of the coatings were obtained from indentation load-displacement data. Here, a positive correlation was found (Fig. 2). As the Young's modulus increases, the hardness increases degressively. The coating thickness was measured by means of scanning electron microscopy (SEM) of cross-sections of the coated inserts. A total of three measurements were carried out on the flank and the rake face as well as the on the cutting edge rounding.

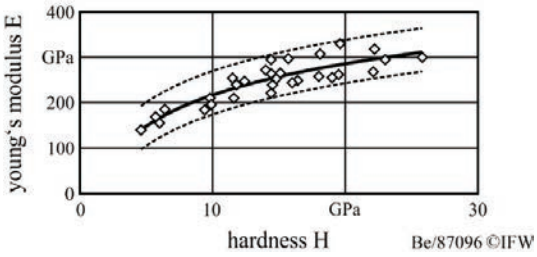

Fig. 2. Relationship between hardness and Young's modulus.

The 3D areal roughness parameters of the coated inserts were measured using the confocal microscope Nanofocus µSurf. In order to characterize the surface topography of the coated inserts the maximum height of the surface Sz and the arithmetical mean height of the surface Sa were determined. Since these parameters involve only the statistical distribution of height values along the z axis, additional functional parameters were calculated from the material ratio curve. This curve corresponds to the cumulative probability density function of the surface profile's height and can be calculated by integrating the profile trace. Here, Sk represents the core roughness of the surface over which a load may be distributed after the roughness peaks of the surface have been removed. Fig. 3 illustrates the dependency between the coating thickness t_c and the core roughness depth Sk. It becomes clear, that the

core roughness depth increases with increasing coating thickness. Furthermore, compared to the rake face the flank face is characterized by a significantly higher core roughness depth.

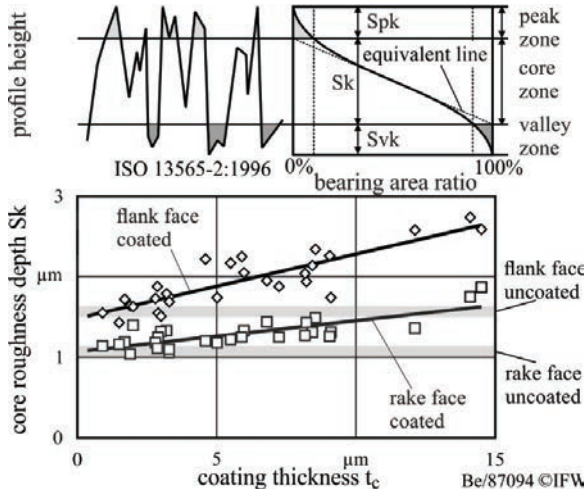

Fig. 3. Core roughness depth Sk in dependence of the coating thickness t_c.

4. Experimental setup

Experimental orthogonal turning tests were carried out on the CNC vertical lathe Gildemeister CTV400 without coolant. Tubes with a diameter of 100 mm and a wall thickness of 3 mm were machined (cutting width b = 3 mm). AISI 4140 (225 HV) was used as workpiece material. A constant cutting speed of v_c = 150 m/min and uncut chip thickness of h = 0.1 mm were used in the investigations. A rake angle of γ = -6° and a clearance angle of α = 6° were applied. In order to stabilize the cutting wedge and to avoid edge chipping an average cutting edge rounding of $\overline{S}$ = 30 µm was used [8]. Process forces were measured by a 3-component-dynamometer Kistler 9129AA. For the detection of the width of flank wear land VB_{max} a digital microscope Keyence VHX-600 was used. The delaminated coating volume V_D was determined with the confocal microscope Nanofocus µSurf. Within this work, a total of 29 different CrAlN-based coatings were investigated. These differed in terms of hardness, Young's modulus, chemical composition and coating thickness.

5. Finite element modeling

For the simulations, the commercial software SFTC Deform 2D 11.0.2 is applied. In order to calculate the stress distribution, a total of three simulation steps were performed. The procedure is illustrated in Fig. 4. The first simulation step is based on a thermomechanical coupled 2-dimensional FEM simulation of the orthogonal cut with plain strain conditions. In order to obtain a steady state in terms of process forces, contact length, chip thickness, shear angle and temperature distribution in the primary heat generation zones the process is simulated with an implicit Lagrangian formulation and continuous remeshing. Mesh density windows are applied to control the element size in front of the cutting edge and at the tool tip. Remeshing is induced when the interference depth between tool and workpiece elements reaches 1/3 of the smallest element or the Jacobian determinant becomes negative, which corresponds to a high distortion of the elements due to strong deformation of the workpiece material.

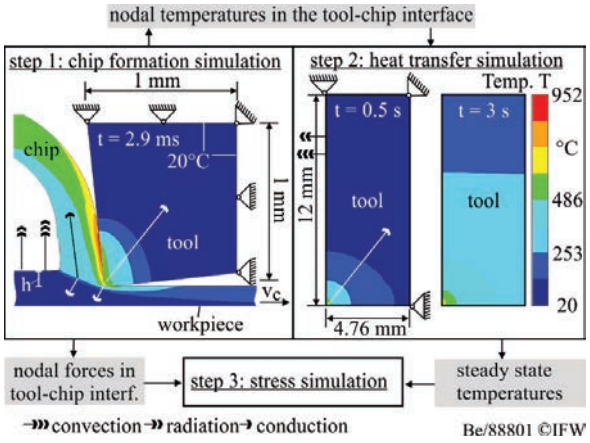

Fig. 4. Experimental setup.

For the workpiece elastoplastic material behavior was assumed. The tool was defined as a rigid body. In the first step, only a small area of 1 mm² is used to reduce computation time. In order to ensure a constant heat flow in the direction of the free surfaces of the tool a set temperature of 20 °C is applied to all boundary nodes. This ensures a constant temperature gradient and therefore a continuous heat transfer to the outer edges of the tool. Based on the nodal temperatures of the boundary elements of the tool at the end of the Lagrangian simulation a heat transfer simulation is applied to reach the thermal steady state inside the cutting tool. In order to avoid errors in the calculation of the temperature distribution, the dimensions of the tool were adapted according to the experimental investigation. For both simulation steps the heat transport within the objects takes place by means of thermal conduction, depending on the material-dependent heat conduction coefficient and the local temperature gradient. The heat transfer to the atmosphere is defined by convection and heat radiation. After reaching the thermal equilibrium in the tool, the previously determined nodal forces are used as boundary conditions for the stress calculation. In this step, a linear elastic behavior is assumed for the tool. The coating is modeled using a structured mesh consisting of quadrilateral elements with regular connectivity. This results in better convergence and a higher space efficiency compared to unstructured meshes.

The Johnson-Cook constitutive material model (Eq. 1) is used to simulate the strain ε, strain rate $\dot{\varepsilon}$ and temperature T dependent flow stress of the workpiece.

$$\sigma = \left(A + B\varepsilon^n\right)\cdot\left(1 + C\cdot\ln\left(\frac{\dot{\varepsilon}}{\dot{\varepsilon}_0}\right)\right)\cdot\left(1 - \left(\frac{T - T_{room}}{T_{melt} - T_{room}}\right)\right)^m \quad (1)$$

A is the initial yield stress (MPa) and B is the hardening modulus (MPa). C defines the strain rate dependency, n is the work hardening exponent and m is the thermal softening coefficient. T_{melt} is the melting temperature and T_{room} is the room temperature. These material constants have a significant influence on chip formation and tool load. Therefore, different parameter sets for AISI 4140 from the literature were compared with the experimental results. The applied parameter sets are summarized in Table 2.

Table 2. Johnson-Cook material constants for AISI 4140 by various authors.

Set	Author	A [MPa]	B [MPa]	C [-]	n [-]	m [-]	$\dot{\varepsilon}_0$ [1/s]
1	Krajinovic [9]	600	643	0.0037	0.041	0.957	0.001
2	Abouridouane [10]	510	480	0.018	0.25	1.46	0.002
3	Moufki [11]	612	436	0.008	0.15	1.46	0.001
4	Lee [12]	1057	755	0.014	0.15	1.46	1
5	Molinari [13]	612	436	0.008	0.15	1.46	0.000577
6	Grolleau [14]	598	768	0.0137	0.2092	0.807	0.001
7	Agmell [15]	594	615	0.023	0.142	1.1611	1
8	Pantale [16]	806	614	0.0089	0.168	1	1
9	Pantale [17]	595	580	0.023	0.133	1.03	1

Furthermore, temperature dependent thermomechanical material properties of AISI 4140 are used. The required data was taken from the Deform database and is shown in Table 3.

Table 3. Workpiece properties.

Temperature T	[°C]	20	100	600	1500
Young's modulus E	[GPa]	212	207	164	70
Poisson's ratio ν	[-]	0.3	0,3	0,3	0,3
Specific heat capacity c_p	[J/kg K]	361	389	610	610
Thermal conductivity λ	[W/m K]	41.7	43.4	34.1	34.1
Thermal expansion coeff. α	[10^{-5}/K]	1.19	1.25	1.49	1.49

The simulation model was calibrated with respect to the experimental results, shown in Table 4. Despite the variety of different coating properties used in the experiment, no significant influence of these properties on the initial process forces as well as the apparent friction factor μ_{app} (Eq. 2) and the measured deformed chip thickness h′ was determined.

$$\mu_{app} = \tan\left(\tan^{-1}\left(\frac{F_f}{F_c} \right) + \gamma \right) \tag{2}$$

Table 4. Experimental results.

		$\bar{x}$	s
Cutting force F_c	[N]	904	17
Feed force F_f	[N]	790	30
Apparent friction coef. μ_{app}	[-]	0.704	0.017
Chip thickness h′	[µm]	0.225	0.03

Therefore, in order to identify a suitable material model, the average value of the experimentally measured apparent coefficient of friction $\bar{\mu}_{app}$ was applied. The comparison of the different parameter sets shows that the material model has a significant influence on the deformed chip thickness and the process forces (Fig. 5). For the subsequent investigations, parameter set 9 is used. According to Coulomb's friction model, the tangential stress is proportional to the normal stress in the contact area of two bodies, which can be described by the coefficient of friction μ (Eq. 3).

$$\tau_f = \mu \cdot \sigma_n \tag{3}$$

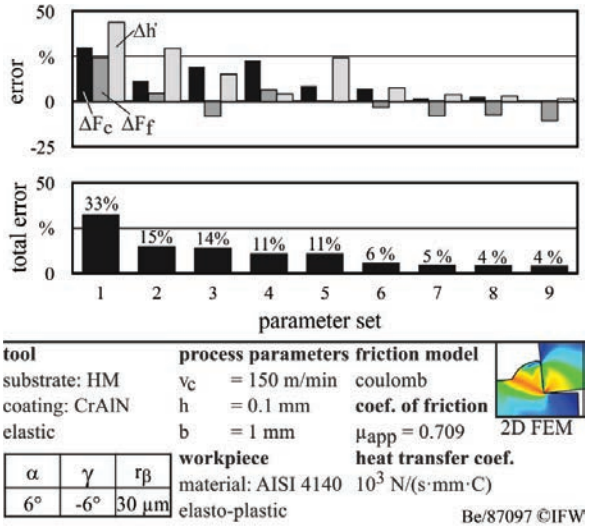

Fig. 5. Calculation error using different JC parameter sets for AISI 4140.

Due to its simplicity this model is often implemented in chip formation simulations. However, if the tangential stress at the tool-chip contact reaches the yield stress of the softer material, the resulting shear stresses can no longer increase linearly and the area of validity of the Coulomb model ends. The friction behavior at high normal stresses can be described by the shear friction model (Eq. 4). Contrary to the Coulomb friction, the tangential forces caused by friction are not proportional to the normal forces, but are proportional to the flow stress k of the softer of the two friction partners. The friction factor m can vary between 0 and 1, where m = 0 is equivalent to perfect lubrication and m = 1 corresponds to full adhesion.

$$\tau_f = m \cdot k \tag{4}$$

Compared to the coulomb friction model the shear friction model underestimates the shear stress τ_f for low normal stresses σ_n. Therefore a nonlinear friction model is used (Eq. 5 and 6).

$$\tau_f = m \cdot k \quad \text{if} \quad \mu \cdot \sigma_n \geq m \cdot k \tag{5}$$

$$\tau_f = \mu_{app} \cdot \sigma_n \quad \text{if} \quad \mu \cdot \sigma_n < m \cdot k \tag{6}$$

While μ is set to 0.7 for all simulations, different values for the shear friction factor m are applied, representing a different adhesive behavior. The results are depicted in Fig. 6. As the shear friction factor decreases, the maximum temperature increases on the cutting edge rounding and along the rake face. This can be attributed to the increased sliding velocity of the chip due to less adhesive behavior. In addition, the contact length increases with the shear factor, which leads to an increase of the process forces.

In order to analyze the tool load in dependence of the layer properties, the hybrid model with m = 1 and μ = 0.7 was applied. The fundamental coating properties of CrAlN are varied with respect to physical and technological limits,

which are taken from the literature (Table 5).

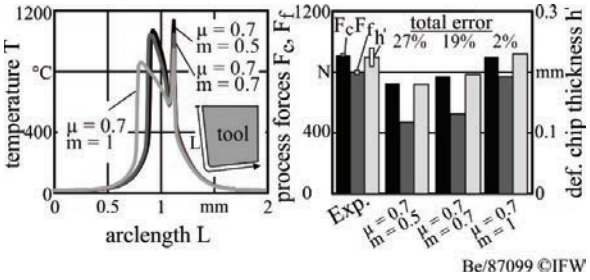

Fig. 6. Influence of the shear friction factor m on the thermomechanical load.

The variation of the coating properties is based on the one-factor-at-a-time method, each factor having three levels. According to the experiments, the coating thickness was varied on four levels (1, 5, 10, 15 µm).

Table 5. Coating properties

		Lowest value	Highest value
Young's modulus E	[GPa]	241 [18]	550 [19]
Poisson's ratio ν	[-]	1.72 [20]	0.268 [20]
Specific heat capacity c_p	[J/kg K]	465[1]	738[2]
Thermal conductivity λ	[W/m K]	2.8 [21]	4.5 [21]
Thermal expansion coef. α	[10^{-6}/K]	5.3[1] [22]	6.0[2] [23]

[1] value for AlN, [2] value for CrN

6. Results

One of the main influencing factors on the thermo-mechanical load is the coating thickness (Fig. 7). At higher coating thicknesses, higher temperatures occur in the contact area and orthogonal to the rake face. This can be attributed to the significantly lower thermal conductivity of the coating compared to the substrate. Furthermore, the temperature gradient between the coating and the substrate increases with higher coating thickness. In the contact area between the chip and the tool the lowest temperatures occur independently of the applied coating thickness on the cutting edge rounding. This is related to the lower sliding velocity of the deformed workpiece material, caused by the material separation in front of the cutting edge rounding.

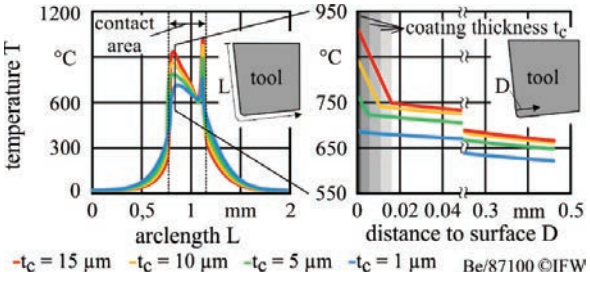

Fig. 7. Influence of the coating thickness on the simulated thermal load.

As depicted in Fig. 8, the probability for coating delamination increases significantly for a coating thickness above 5 µm. Therefore, this value is referred to as critical coating thickness. Coating delamination occurs, in particular, in the region of the cutting edge rounding (Fig. 8A). According to the simulation, higher effective von Mises stresses σ_{eff} occur in the coating-substrate interface, which may lead to a higher probability to delamination wear (Fig. 8B).

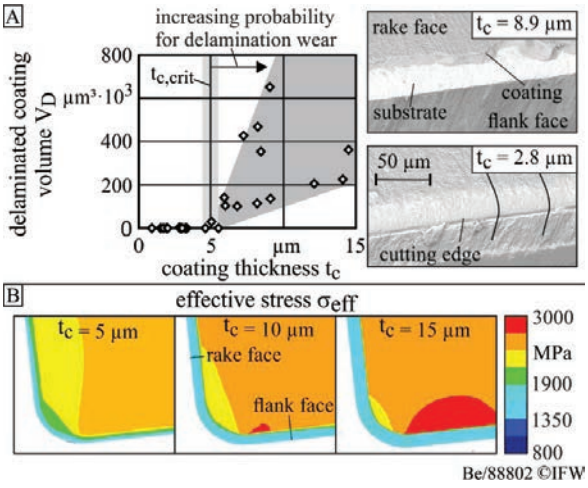

Fig. 8. Influence of the coating thickness on delamination wear.

Referring to Fig. 9, which shows the influence of the elastic coating properties on the von Mises stresses and the minimum principle stresses, the stress distribution in the coating is mainly influenced by its Young's modulus. Increasing the Young's modulus induces higher effective von Mises stresses as well as increasing minimum principle stresses. This is associated with the higher resistance to elastic deformation. A similar effect is obtained by increasing the thermal expansion coefficient and Poisson's ratio. However, the stress distribution in the substrate is not affected.

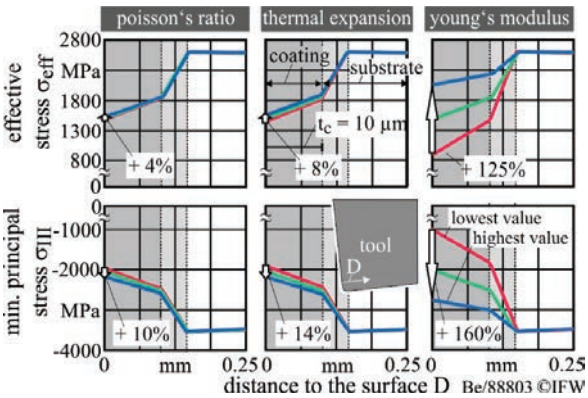

Fig. 9. Influence of the elastic properties on the stress distribution orthogonal to the rake face.

Taking into account the technological limits of CrAlN-based coatings, the thermal conductivity and the specific heat capacity show no significant effects on the coating load and the resulting stresses. Temperature changes of up to 30 °C and stress changes of less than 4 % were determined. However, it should be noted that the thermal conductivity is significantly lower compared to other coatings, resulting in an increased

heat accumulation in the coating.

As shown in Fig. 10, the width of flank wear land VB correlates with the measured core roughness depth Sk. This can be attributed to the increased load carrying capability of the surface at a lower core roughness depth.

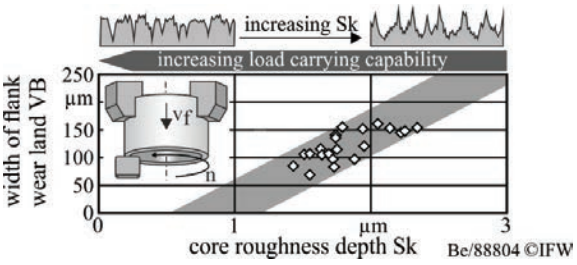

Fig. 10. Influence of the core roughness depth Sk on the flank face

7. Conclusion

Within the present work, the impact of the coating properties on the coating load and the resulting stress distribution in the tool was analyzed. The following conclusions can be drawn:

- The initial thermomechanical load on the cutting tool surface is mainly influenced by the coating thickness and the adhesion behavior.
- The Young's modulus significantly influences the stresses in the coating. The stresses within the substrate are not affected.
- The increased probability for coating delamination at high coating thicknesses can be linked to increased interface stresses
- With increasing coating thickness, a heat accumulation results due to the low thermal conductivity. Taking into account the temperature dependent hardness, this may lead to a decrease of the resistance to abrasive wear.
- High core roughness depths on the flank face lead to higher flank wear.

For future research, it is necessary to not only determine the influence of the coating properties on the thermomechanical load, but also to understand the relationship between the process conditions and the resulting wear, taking into account the progressive wear-related change of the tool geometry in the simulation.

Acknowledgements

The authors thank the German Research Foundation (DFG) for the financial support within the project "Simulationsoptimierte PVD-Beschichtungen" and the Ceratizit S.A., Luxembourg, for the cooperation.

References

[1] Bouzakis KD, Michailidis N, Skordaris G, Bouzakis E, Biermann D, M'Saoubi R. Cutting with coated tools: Coating technologies, characterization methods and performance optimization. CIRP Annals – Manufacturing Technology 2012; 61: 703-723.

[2] Abele E, Schramm B, Scheerer H. Dry machining using novel chromium based coatings. Advances in Production Engineering & Management 2008; 3: 141-148.

[3] Ding XZ, Zheng XT, Liu YC, Fang FZ, Lim GC. $Cr_{1-x}Al_xN$ coatings deposited by lateral rotating cathode arc for high speed machining applications. Thin Solid Films 2008; 1710-1715.

[4] Endrino JL, Fox-Rabinovich GS, Gey C. Hard AlTiN, AlCrN PVD coatings for machining of austenitic stainless steel. Surface & Coatings Technology 2006; 200: 6840-6845.

[5] Kone F, Czarnota C, Haddag B, Nouari M. Finite element modelling of the thermo-mechanical behavior of coating under extreme contact loading in dry machining. Surface & Coatings Technology 2011; 205: 3559-3566.

[6] Bouzakis KD, Vidakis N, Kallikinidis D, Leyendecker T, Erkens G, Wenke R, Fuss HG. Fatigue failure mechanisms of multi- and monolayer physically vapour-deposited coatings in interrupted cutting processes. Surface & Coatings Technology 1998; 108: 526-534.

[7] Özel T, Sima M, Srivastava AK, Kaftanoglu B. Investigation on the effects of multi-layered coated inserts in machining Ti-6Al-4V alloy with experiments and finite element simulations. CIRP Annals – Manufacturing Technology 2010; 59: 77-82.

[8] Denkena B, Biermann D. Cutting Edge Geometries. CIRP Annals – Manufacturing Technology 2014; 63(2): 631-653.

[9] Krajinović K, Daves W, Tkadletz M, Teppernegg T, Klünsner T, Schalk N, Mitterer C, Tritremmel C, Ecker W, Czettl C. Finite element study of the influence of hard coatings on hard metal tool loading during milling. Surface and Coatings Technology 2016; 304: 134-141.

[10] Abouridouane M, Klocke F, Döbbeler B. Analytical temperature prediction for cutting steel. CIRP Annals – Manufacturing Technology 2016; 65: 77-80.

[11] Moufki A, Devillez A, Segreti M, Dudzinski D. A semi-analytical model of non-linear vibrations in orthogonal cutting and experimental validation. International Journal of Machine Tools Manufacturing 2006; 46: 436-449.

[12] Lee TH. Development of a Theoretical Model to Predict Cutting Forces for Hard Machining. International Journal of Precision Engineering and Manufacturing 2011; 12(5): 775-782.

[13] Molinari A, Moufki A, Dudzinski, D. Study on behaviour of 42CrMo4 Steel. Final technical report, CREAS Ascometal, 1997.

[14] Grolleau V. Approche de la validation expérimentale des simulations numériques de la coupe avec prise en compte des phénomènes locaux à l'arête de l'outil. Ph.D. thesis, Ecole Centrale de Nantes; 1996.

[15] Agmell M, Ahadi A, Stahl JE. Identification of plasticity constants from orthogonal cutting and inverse analysis. Mechanics of Materials 2014; 77: 43-51.

[16] Pantale O. Virtual prototyping platform for numerical simulation in large thermomechanical transformations. Ph.D. thesis, Institut National Polytechnique de Toulouse; 2005.

[17] Pantale O, Bacaria JL, Dalverny O. 2D and 3D numerical models of metal cutting with damage effects. Computer Methods in Applied Mechanics and Engineering 2004; 193: 4383-4399.

[18] Chen HW, Chan YC, Lee JW, Duh JG. Oxidation resistance of nanocomposite CrAlSiN under long-time heat treatment. Surface & Coatings Technology 2011; 206: 1571-1576.

[19] Bouzakis KD, Michailidis N, Gerardis S, Katirtzoglou G, Lili E, Pappa M, Brizuela M, Garcia-Luis A, Cremer R. Correlation of the impact resistance of variously doped CrAlN PVD coatings with their cutting performance in milling aerospace alloys. Surface & Coatings Technologie 2008; 203(5): 781-785.

[20] Zhou L, Holec D, Mayrhofer PH. First principles study of elastic properties of Cr-Al-N. Journal of Applied Physics 2013; 113(4): 1-8.

[21] Tlili B, Mustapha N, Nouveau C, Benlatreche Y, Guillemot G, Lambertin M. Correlation between thermal properties and aluminum fractions in CrAlN layers deposited by PVD technique. Vacuum 2010; 84(9): 1067-1074.

[22] Yim WM, Paff RJ. Thermal Expansion of AlN, sapphire, and silicon. Journal of Applied Physics 1974; 45(3): 1456-1457.

[23] Gall D, Shin CS, Spila T, Odén M, Senna MJH, Greene JE; Petrov I. Growth of single-crystal CrN on MgO(001): Effects of low-energy ion-irradiation on surface morphological evolution and physical properties. Journal of Applied Physics 2002; 91(6): 3589-359.